Colloids and Surfaces B: Biointerfaces 203 (2021) 111753

Contents lists available at ScienceDirect

Colloids and Surfaces B: Biointerfaces

journal homepage: www.elsevier.com/locate/colsurfb

Bicontinuous cubic liquid crystalline phase nanoparticles stabilized by softwood hemicellulose

Polina Naidjonoka [a,*,1], Marco Fornasier [a,b,*,1], David Pålsson [a,1], Gregor Rudolph [c], Basel Al-Rudainy [c], Sergio Murgia [d], Tommy Nylander [a,e,f]

[a] Division of Physical Chemistry, Department of Chemistry, Lund University, P.O. Box 124, Lund, SE-221 00, Sweden
[b] Department of Chemical and Geological Sciences, University of Cagliari, s.s 554 bivio Sestu, Monserrato, I-09042, Italy
[c] Department of Chemical Engineering, Lund University, SE-221 00, Lund, Sweden
[d] Department of Life and Environmental Sciences, University of Cagliari, via Ospedale 72, Cagliari, I-09124, Italy
[e] NanoLund, Lund University, Lund, Sweden
[f] Lund Institute of Advanced Neutron and X-ray Science LINXS, Lund, Sweden

ARTICLE INFO

Keywords:
Cubosomes
Stabilizer
Hemicellulose
Lignin

ABSTRACT

The colloidal stability of lipid based cubosomes, aqueous dispersion of inverse bicontinuous cubic phase, can be significantly increased by a stabilizer. The most commonly used stabilizers are non-ionic tri-block copolymers, poloxamers, which adsorb at the lipid-water interface and hence sterically stabilize the dispersion. One of the challenges with these synthetic polymers is the effect on the internal structure of the cubosomes and the potential toxicity when these nanoparticles are applied as nanomedicine platforms. The natural polysaccharide, softwood hemicellulose, has been proved to be an excellent stabilizer for oil-in-water emulsions, partially due to the presence of hydrophobic lignin in the extract which to some extent is associated to hemicellulose.

Herein, we reported for the first time cubosomes stabilized by two types of softwood hemicelluloses, where one is extracted through thermomechanical pulping (TMP, low lignin content) and the other obtained from sodium-based sulfite liquor (SSL, high lignin content). The effect of the two hemicellulose samples on the colloidal stability and structure of monoolein-based cubosomes have been investigated *via* DLS, SAXS, AFM and cryo-TEM. The data obtained suggest that both types of the hemicelluloses stabilize monoolein (GMO) based cubosomes in water without significantly affecting their size, morphology and inner structure. SSL-extracted hemicellulose yields the most stable cubosomes, likely due to the higher content of lignin in comparison to TMP-stabilized ones. In addition, the stability of these particles was tested under physiological conditions relevant to possible application as drug carriers.

1. Introduction

Non-lamellar Lipid Liquid Crystalline Nanoparticles (LLCNPs) have been widely studied in the last decades due to their intriguing structure and morphology. Examples of these kind of aggregates are cubosomes [1,2], hexosomes [2,3] and the dispersion of sponge phase (spongosomes) [4,5].

Cubosomes are dispersions of an inverse bicontinuous cubic phase in which a curved non-intersecting bilayer forms two continuous and unconnected system water channels. The curved bilayer can be described by an infinite periodic minimal surface (IPMS), such as the primitive (Im3m), the gyroid (Ia3d) and the double-diamond (Pn3m). Monoolein (GMO) and phytantriol are among the most studied lipids that form cubic phases, [1,6] nevertheless other lipids can be adopted to formulate the particles [7].

The preparation of the LLCNPs is based on a top-down, bottom-up or microfluidic approach. Lipid Liquid Crystalline (LLC) cubic bulk phase can be fragmented with *e.g.* homogenization involving high-energy input often with the help of an emulsifier. The most common bottom-up method yields the aggregates *via* dissolution of the lipid components in solvent and thereafter mixing of the lipid solution with an aqueous solution of additives to obtain the dispersion.

* Corresponding authors at: Division of Physical Chemistry, Department of Chemistry, Lund University, P.O. Box 124, Lund, SE-221 00, Sweden.
E-mail addresses: polina.naidjonoka@fkem1.lu.se (P. Naidjonoka), mfornasier@unica.it (M. Fornasier).
[1] These authors equally contributed to this work.

https://doi.org/10.1016/j.colsurfb.2021.111753
Received 29 October 2020; Received in revised form 4 March 2021; Accepted 3 April 2021
Available online 7 April 2021

Colloidally stable cubosome dispersions require a stabilizing agent, such as tri-block copolymers, to a larger extent than their lamellar counterpart, liposomes. Here, Poloxamers (poly(ethylene oxide)-poly (propylene oxide)-poly(ethylene oxide)), *i.e.* Pluronics F127 and F108, are the most common stabilizers, where the hydrophobic PPO moiety interacts with the lipid bilayer and the PEO units form a hydrophilic corona that prevents NPs from aggregating.

The biocompatibility and biodegradability of the components of the formulations are crucial parameters for application of cubosomes in drug delivery and imaging [8–13]. Although the GMO-based carriers are less cytotoxic compared to those based on phytantriol [1,6], the intrinsic cytotoxicity of the stabilizer could prevent the application of the system [14]. Therefore, stabilizing the cubic dispersion and at the same time providing a "safe" formulation can be challenging.

Recently, a polyphosphoester (PPE) tri-block copolymer, a structural analog of Pluronic F127, was shown to be able to stabilize GMO-based cubosomes [15]. Biocompatibility assay on Human umbilical vein endothelial cells (HUVEC) and blood cells showed that the PPE-stabilized NPs were less cytotoxic at the same concentration in comparison to the cubosomes stabilized with Pluronic F127. These new formulations were also shown to have less tendency to activate the complement system, which our body employs to remove anything foreign from the blood stream.

The cytotoxic effect can be reduced by mimicking natural molecular structures and thereby improving the efficacy of the therapy. For this reason, natural polysaccharides are of great interest as potential nanoparticle stabilizers. In addition, they can remain functional as stabilizers over a relatively broad range of temperatures and pH. However, lack of clear and structured amphiphilic character brings a variety of challenges to the table. Several studies have been published where monoolein cubosomes have been stabilized by different polysaccharides like starch and cellulose [16–18]. These polysaccharides were, however, modified by introducing hydrophobic groups in their structure. This is a promising alternative to commonly used Pluronic F127 that is believed to have some unwanted physiological side effects when ingested or inhaled, [18] and also has shown to affect the internal structure of monoolein based cubosomes. Here we have explored the stabilizing potential of hemicellulose that along with cellulose and lignin is one of the main polymer constituents of plant cell walls. Hemicelluloses are heteropolysaccharides that vary in structure and size depending on the plant type. Lignin, on the other hand, is a highly hydrophobic group of aromatic polyphenol compounds that are strongly associated with hemicelluloses and help to provide mechanical strength to the cell walls [19]. Hemicelluloses have been shown to have excellent emulsifying properties in several applications [20–25].

The chemical composition of hemicellulose is dependent on the plant type and is often affected by the extraction method. A great variety of methods have been developed in order to obtain high purity extracts. However, one of the biggest challenges still remains the removal of lignin since it is covalently bound to hemicellulose sugar groups *via* glycosidic, ester or ether bonds [24]. Interestingly, when it comes to stabilizing oil in water emulsions, lignin plays an impartial role as it is believed to interact with the hydrophobic moiety of lipids and anchor hemicellulose chains on the interface. Hemicellulose in turn provides steric stabilization mechanism due to chains with high molecular weight.

The most abundant hemicellulose in spruce and pine is galactoglucomannan (GGM). It accounts for 25–35 % of dry wood mass [26,27]. Galactoglucomannans, often acetylated, have a linear (1→4)-linked β-D-mannopyranosyl (Man*p*) backbone partially substituted with (1→4)-linked β-D-glucopyranosyl (Glc*p*) units and α-galactopyranosyl (Gal*p*) side groups that are (1→6)-linked to the backbone [28,29]. Softwood hemicellulose has been used as a feeding stock for ruminants without showing adverse effects and even demonstrated prebiotic properties in healthy mice [30,31]. In addition, several galactomannans like konjac and guar which are similar in structure to softwood hemicellulose (galactoglucomannan) are widely used as food constituents and have been shown not to be carcinogenic to rats and mice [32].

In this study, we investigate the ability of two different softwood hemicellulose preparations to stabilize monoolein cubic nanoparticles. One is the TMP (thermomechanical pulping) hemicellulose, which has been isolated from thermomechanical pulp and contains a very low amount of lignin, whereas the SSL (spent-sulfite-liquor) preparation originates from a sodium-based sulfite liquor with a relatively high lignin concentration. The effect of these stabilizing agents on the structure, morphology and colloidal stability of the lipid based cubosomes was studied in order to identify their possible application as components to prepare future drug carriers.

2. Experimental section

2.1. Materials

The main component of the cubosomes, glycerol monooleate (MO, 1-monooleoylglycerol, RYLO MG 19 PHARMA, 98.1 wt% monoglycerides) was kindly provided by Danisco A/S (now Dupont, Denmark). Fresh distilled water purified using a Milli-Q® water purification system (MerckMillipore, Darmstadt, Germany) was used for preparing each sample and it was filtered with a 0.22 μm pore size hydrophilic filter prior to any use. Chloroform (99.8 % purity) and phosphate buffered saline (PBS) tablets were purchased from Sigma-Aldrich (0.01 M phosphate buffer, 0.0027 M potassium chloride and 0.137 M sodium chloride).

The TMP and SSL hemicellulose sample was obtained from Stora Enso Kvarnsvedens bruk (Kvarnsveden, Sweden) and Domsjö Fabriker (Örnsköldsvik, Sweden), respectively. Purification of both samples was done in-house at the Department of Chemical Engineering at Lund University. TMP extract was purified according to the procedures reported by Thuvander et al. [33] and Zasadowski et al. [34] and characterized according to the National Renewable Energy Laboratory (NREL) procedure. [35] Details of the extraction procedure and analysis of the SSL sample can be found at Al-Rudainy et al. [36] Table 1 shows a summary of the main components present in each of the samples. The MW of GGM can generally be expected to be around 15−24 kDa in spruce, [26,37] but even much bigger MW of up to 490 kDa has been reported [38]. The MW depends on the analysis method and to some extent on the pulping process. However for GGM from TMP [39] and SSL [36] the MW can be expected to be similar and in the mentioned range.

Table 1
The chemical composition of the TMP and SSL hemicellulose extracts shown as weight percentage of total dry solids (TDS). [36] Acidic components were not determined for TMP extract indicated as n.d.

	wt % of TDS	
	TMP	SSL
Ash	0	2.02
Lignin	1.26	7.3
Carbohydrates		
Arabinose	0	1.11
Galactose	10.4	18.7
Glucose	8.8	14.85
Xylose	4.7	7.05
Mannose	76	30.78
Cellobiose	n.d.	1.14
Lactic acid	n.d.	1.68
Acetic acid	n.d.	3.99
Formic acid	n.d.	1.63
Levulinic acid	n.d.	2.17
Furfural	n.d.	1.25
Hydroxymethylfurfural	n.d.	0.62

2.2. Methods

2.2.1. Sample preparation

Cubosome formulations were prepared by first dissolving 10 mg of monoolein in 1 mL of chloroform in a vial. The chloroform was then evaporated under a gentle stream of nitrogen to yield a lipid film, which was left to dry under vacuum overnight at room temperature to remove any trace of chloroform. 1 mL of GGM aqueous solution with a concentration of 3 mg mL^{-1} was then added to the vial with the monoolein film. The sample was vortexed for a few seconds and left to equilibrate at room temperature for one hour. After that, the mixture was placed in an ice bath and sonicated with a tip sonicator (equipped with a controller Sonics Vibra Cells, both from Chemical Instruments AB, Sweden) for 15 min at 70 % amplitude with 10 s pulses in 10 s intervals. The samples were characterized within 48 h after preparation.

2.2.2. Dynamic light scattering (DLS) and electrophoretic mobility (EM)

Dynamic light scattering experiments were performed on a Zetasizer Nano ZS (Malvern Instruments Ltd, Worshestershire, UK) at a set angle of 173° using the non-invasive backscatter technology. The instrument was equipped with a 4 mW He-Ne laser with a 632.8 nm wavelength and an Avalanche photodiode detection unit. The electrophoretic mobility measurements were performed using M3-PALS technology at 13°. The obtained correlation functions were analyzed using the cumulants method available in the Malvern software.

The cubosome formulations were diluted 500 times with either Milli-Q water or PBS buffer, placed in the Zetasizer measurement cell and equilibrated at 25 °C for 2 min before starting the measurement.

2.2.3. Small angle X-ray scattering (SAXS)

SAXS measurements were performed at the SAXSLab instrument (JJ-Xray, Denmark) available at Lund University. The instrument was equipped with a 30 W Cu X-RAY TUBE for GeniX 3D and a 2D 300 K Pilatus detector (Dectris). The X-ray wavelength was 1.54 $Å^{-1}$ and the sample-to-detector distance was 480 mm, yielding a q-range of 0.012 – 0.67 $Å^{-1}$. The measurements were recorded at 25 °C. The temperature was controlled using a Julabo T Controller CF41 from Julabo Labortechnik GmbH (Germany).

The magnitude of the scattering vector is defined by $q = 4\pi/(\lambda \cdot \sin\theta)$, where the wavelength λ equals to 1.54 Å, Cu Kα wavelength, and θ is half of the scattering angle.

The repeat distance or d spacing was obtained using the following expression:

$$d = \frac{2\pi}{q} \quad (1)$$

Then, the cubic phase lattice parameter (a) is given by eq. 2:

$$a = d \cdot \sqrt{h^2 + k^2 + l^2} \quad (2)$$

Here, h, k and l are the Miller indexes that describe the crystalline planes into the liquid crystalline lattice. The lattice parameter was used to estimate the water channel radius (r_w) of the bicontinuous cubic phase (eq. 3) [40]:

$$r_w = (a - l) \cdot \sqrt{\frac{A_0}{-2\pi\chi}} \quad (3)$$

where χ and A_0 are the Euler characteristic and the surface area of the IPMS geometry (Pn3m, $\chi = -2$, $A_0 = 1.919$), respectively, and l is the MO hydrophobic chain length at 25 °C (17 Å).

The formulations in PBS buffer were prepared by diluting the aqueous stock of cubosome dispersion 10 times with the buffer.

2.2.4. Cryogenic-TEM (cryo-TEM)

A 4 μL drop of the formulations at the initial concentration was placed on a lacey carbon coated formvar grid (Ted Pella Inc, Redding, CA, USA). A thin film was then created by gently blotting the grid with a filter paper. After that the grid was prepared for imaging using an automatic plunge-freezer system (Leica Em GP, Leica Microsystems, Wetzlar, Germany). The environmental chamber was operated at 25 °C and 90 % relative humidity to prevent evaporation from the sample. The specimen was vitrified by rapidly plunging the grid into liquid ethane (−183 °C) and the samples were stored in liquid nitrogen (−196 °C) and transferred into the microscope using a cryo transfer tomography holder (Fischione, Model 2550, E.A. Fischione Instruments, Inc., Corporate Circle Export, PA, USA). The grids were imaged with a Jeol JEM-2200FS transmission electron microscope (JEOL, Tokyo, Japan) equipped with a field-emission electron source, a cryo-pole piece in the objective lens and an in-column energy filter (omega filter). Zero-loss images were recorded with a bottom-mounted TemCam F416 digital camera (TVIPS-Tietz Video and Image Processing Systems GmbH, Gauting, Germany) using SerialEM under low-dose conditions at an acceleration voltage of 200 kV.

Gwyddion software [41] was used to apply 2D Fourier transform filter to cryo-TEM micrographs and extract lattice parameter.

2.2.5. Atomic Force Microscopy (AFM)

AFM was performed with a Park XE—100 (Park Systems Corp., Suwon, Korea) in a non-contact mode. Samples were probed in a liquid state under ambient conditions. A silicon cantilever with a 3 N/m spring constant and 75 kHz resonance frequency was used. The image analysis was done with the XEI software (Park Systems Corp., Suwon, Korea). A hydrophobized silicon wafer was covered with 90 μL of SSL-NPs formulation and left to adsorb for 4 h before rinsing with Milli-Q water. The wafer with a drop liquid sample was then placed in the AFM liquid cell and Milli-Q water was added, after which the imaging was performed. The preparation was done in this way in order to avoid passing the sample surface film through the air/water interface.

3. Results and discussion

3.1. Preparation of the NPs and their bulk characterization

Formulations stabilized by softwood hemicellulose extracted with two different methods were prepared using ultrasonication and characterized in a similar manner. This approach has been found effective to reduce the size of the aggregates and induce a good size distribution. [1, 6]

After preparation, both formulations appeared homogeneous and milky, however the SSL-stabilized solution was less translucent than the TMP-stabilized sample. The DLS and ζ-potential results, reported in Table 2, indicate that the formulations contain negatively charged, electrostatically stable particles of relatively low polydispersity.

The ζ-potential of the TMP- and SSL- stabilized cubosomes was -37.7 and -49.5 mV, respectively. Negative charge of the nanoparticles could partially be explained by a negative ζ-potential of their respective

Table 2
Apparent average hydrodynamic diameter (d_H), polydispersity index (PdI), derived count rate, as well as phase, lattice parameter (a) and water channel radius (r_w) determined from the SAXS curves for the TMP and SSL formulations. Additionally, ζ-potential and pH of pure TMP and SSL extract, as well as of TMP-NPs and SSL-NPs determined at 25 °C.

Parameters	TMP-NPs	SSL-NPs	TMP	SSL
$d_H \pm$ SD [nm]	151 ± 1	152.2 ± 0.9	–	–
PdI ± SD	0.21 ± 0.02	0.19 ± 0.01	–	–
Derived count rate ± SD	940 ± 3	2032 ± 20	–	–
Phase	Pn3m	Pn3m	–	–
a ± SD [Å]	99.6 ± 0.8	98.7 ± 0.4	–	–
$r_w \pm$ SD [Å]	21.9 ± 0.3	21.6 ± 0.1	–	–
ζ-potential [mV]	−37.7 ± 0.8	−49.5 ± 0.6	−10 ± 1	−14.8 ± 0.2
pH	6.39	6.52	6.44	6.58

hemicellulose extracts (-10 and -14.8 mV for TMP and SSL, respectively). We note that the charge is highly dependent on the extraction method and the purity of the sample. Galactoglucomannans are neutral polysaccharides, the charge is believed to be caused by the presence of acidic groups. [21] The amount of acidic groups present in the TMP sample was not determined, however, the SSL extract contains at least 10 % as shown in Table 1. Interestingly, the apparent negative charge is a common feature of the GMO-based dispersions: this phenomenon is not fully understood, but it has been reported for other lipid formulations stabilized with non-ionic block-copolymers. [15,42] A possible reason could be related to an adsorption of hydroxide ions at the lipid-water interface, resulting in a polarized outer layer surrounding the NPs and an apparent negative surface potential [43]. As already reported in literature with other stabilizers [15] the high negative zeta potential of these types of particles is common and partly contribute to their colloidal stability. Here it should be stressed that the determination of the electrophoretic mobility and the use of these data to calculate a zeta potential assume rather ideal system of spherical particles and relies on defining the slipping plane of the moving objects in an electric field. Absolute quantitative comparison of the values is challenging. Using a stabilizer to prepare the nanoparticles makes them more defined and less polydisperse. For more or less flexible objects as a polymer chain the assumption of spherical objects is not valid. However we can compare the zeta potential of similar entities in solution.

Dispersions formulated with both GGMs exhibited the same size, around 150 nm in diameter, with relatively low polydispersity. Similar size and polydispersity have been previously reported in literature for cubosomes stabilized with different kinds of polymers. [10,15] The intensity of the scattering from the dispersion of the SSL-stabilized NPs is more than twice as high (2032 ± 20) as from the TMP-NPs formulation (940 ± 3), indicating a larger number of particles present in the solution. This finding correlates with the less translucent appearance of the former sample.

It has been previously shown that the presence of lignin in GGM strongly increases their capability to stabilize oil in water emulsions. [20,22–24] Lignin consists of phenolic compounds that are usually associated or even covalently bound to hemicellulose sugar units *via* glycosidic, ester or ether bonds. [24] Due to their hydrophobic nature, phenolic residues interact with the hydrophobic part of the lipids and thus anchor bound hemicellulose chains that in turn provide steric stabilization of the oil/water interface. Consequently, a larger amount of nanoparticles in the sample could be stabilized by the SSL hemicellulose preparation, given its higher content of lignin. In addition, the SSL-NPs have a more negative ζ-potential than the corresponding TMP-NPs. This could contribute to the electrostatic stabilization of the nanoparticles, although it has been suggested that emulsion stabilization with hemicellulose is mainly due to steric repulsion. [44]

SAXS was used to reveal the internal NP structure. Fig. 1 shows SAXS data of the TMP- and SSL-stabilized nanoparticles. Lyotropic GMO-based aqueous dispersions show a rich polymorphism depending on the water content. [45] In excess of water, monoolein is expected to form a Pn3m cubic phase. The presence of a stabilizer can affect monoolein self-assembly as reported by *e.g.* Nakano *et al.* [46] in cubosome dispersions stabilized by Pluronic F127. The interaction between the PPO lipophilic moiety of the stabilizer locally affects the organization of the lipid bilayer, giving two types bicontinuous cubic phases, Im3m and Pn3m, depending on the amount of added stabilizer. In the case of GGM-stabilized formulations, both of the SAXS curves have similar patterns with at least two clearly visible Bragg peaks. The peak positions and profile are characteristic of a Pn3m phase. This is absent in the scattering profiles of the neat GGM extracts (see ESI, Fig. S1), which are well described by the Beaucage model where a fractal morphology with flexible cylinders as building blocks is used to characterize the polymer similar to those we previously reported for highly purified GGM samples. [47] Mannans used here for the stabilization of the nanoparticles are smaller in size but with a comparable degree of chain stiffness as

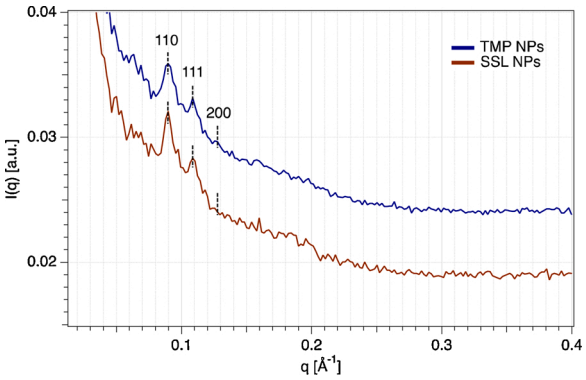

Fig. 1. SAXS curves of the TMP (dark blue) and SSL (brown) nanoparticles. The scattering profile of the TMP was shifted upwards by a factor of 0.01 for clarity. The Miller indices for the Pn3m type of cubic phase are indicated for the corresponding Bragg peaks. The corresponding lattice parameters (a) and water channel radius (r_w) of TMP-NPs and SSL-NPs are shown in Table 1.

evidenced by Kuhn length (see ESI, Table S1), indicating that this is indeed the same type of polymers. The discrepancy in size is likely to be caused by differences in the purification methods. The GGM is covering the surface of the NPs without affecting the internal structure in water. This is in contrast to formulations stabilized with Pluronics. This finding represents a crucial point for a possible application of these aggregates as drug delivery systems. The diffusion coefficient of small hydrophilic molecules in Pn3m bulk phases has been observed to be larger than in Im3m phase, which has been attributed to the higher porosity of the former. [48] Given that the preparation method does not impact the symmetry of the dispersion, we could speculate that the diffusion coefficient trend of molecules within the cubosome's water channels would be similar to the one observed in the two bicontinuous cubic bulk phases.

The lattice parameter and the water channel radius could be determined from the position of the Bragg peaks in the scattering curves. As reported in Table 2, the formulations contain particles with a lattice parameter characteristic to Pn3m phase cubosomes equal to 99.6 Å and 98.7 Å for TMP- and SSL-NPs, respectively.

These values of lattice parameters are in line with the ones already reported for Pluronic-stabilized cubosomes, with no significant difference between the two types of hemicellulose stabilizers. [10,49,50]

In order to assess the morphology of the aggregates, the samples were imaged with cryo-TEM and the results of the two different formulations are shown in Fig. 2. In all of the micrographs, aggregates with a defined internal structure can be observed. In order to confirm internal structure of the nanoparticles, 2D Fourier transform filter was applied to the cryo-TEM images and lattice parameter was extracted. The Fourier transform filtered images of the cubosome internal structure are shown as insets in Fig. 2. Obtained lattice parameters are 89 Å for TMP-NPs and 110 Å for SSL-NPs which agrees well with values extracted based on SAXS patterns. The difference between the lattice parameter obtained with cryo-TEM and SAXS could be related to the fact that the techniques investigate on a different portion of the sample. In the case of SAXS we get a mean value of the lattice parameter of the particles, whereas in cryo-TEM the analysis is restricted to the particles that are actually imaged in that moment. In addition, the lattice parameters obtained by applying 2D Fourier transform filter to cryo-TEM micrographs is based on 2D projection of individual 3D objects that depends on the particular orientation of liquid crystalline domain. In the SAXS data we look at the powder pattern of an assembly of particles. However, the results from both techniques confirm the cubic structures and the lattice parameter values are in the range of what is expected for bicontinuous cubic phase dispersions.

The TMP-NPs sample contains 200–250 nm large cubosomes, in addition to fractal-like aggregates (Fig. 2). Different types of softwood

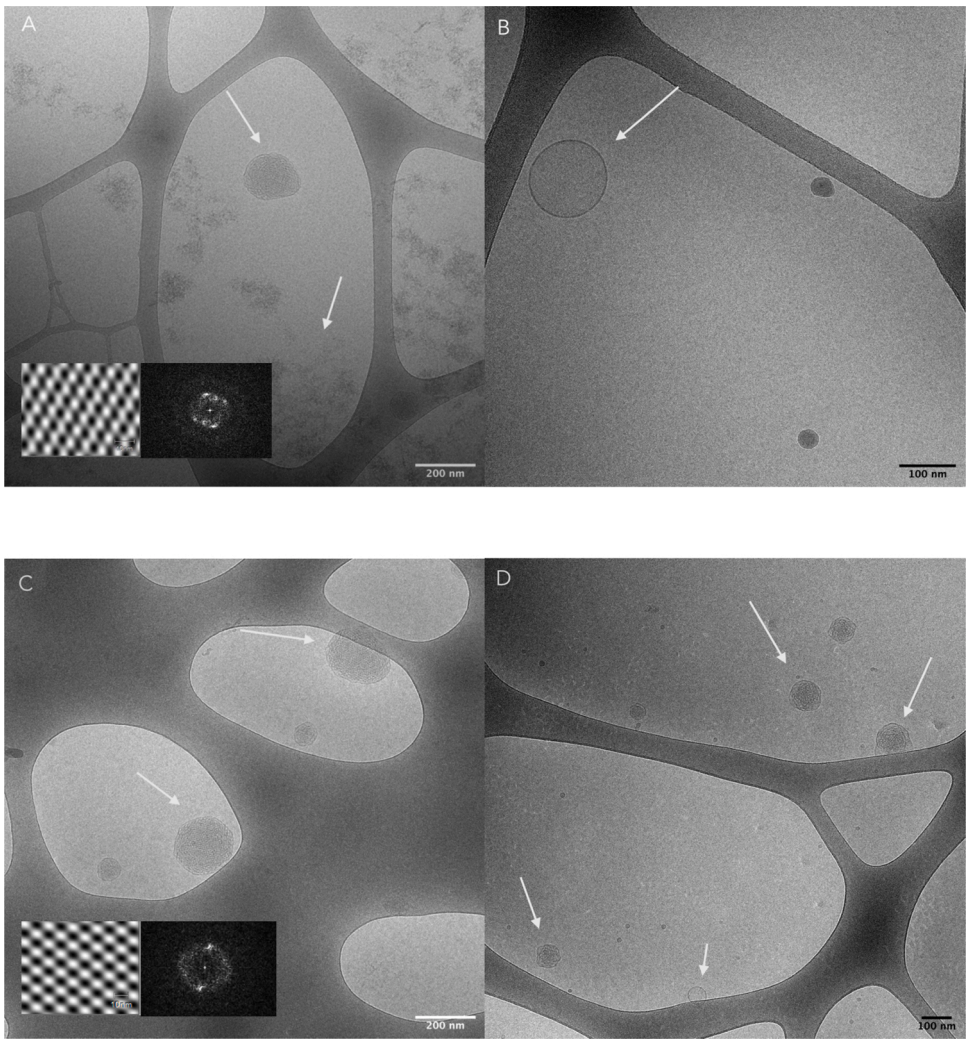

Fig. 2. Cryo-TEM images of TMP-NPs (A and B) and SSL-NPs (C and D) at 10 mg mL^{-1} concentration incubated at 25 °C prior to blotting. Fourier transform as well as the magnified section used for the Fourier transforms are shown as inserts and the results show that the structural periodicity of the nanoparticles consistent with cubic phase mesostructure.

hemicellulose have previously been shown to assemble into similar structures and therefore the aggregates observed in Fig. 2 can be attributed to the excess hemicellulose that is not incorporated in the cubic nanoparticles. [47,51] Additionally, the TMP-stabilized sample contains a small amount of vesicles that are approximately 150 nm large (Fig. 2B).

Fig. 2 (C, D) shows the cryo-TEM images of SSL-stabilized sample. This sample looks more homogenous without the presence of hemicellulose fractal structures. This indicates that most of the hemicellulose is associated with monoolein in the cubosomes. The cubosomes range in diameter from 50 to 200 nm that agrees well with the DLS results. Similar to the TMP-NPs, a low amount of vesicles is present in this sample as well (Fig. 2D).

Since at this concentration, monoolein gives a Pn3m cubic phase with excess water, the presence of vesicles in the sample confirms that hemicellulose interacts with the monoolein lipid bilayer. This result is not surprising, since other studies have highlighted the effect that stabilizers can have on the morphology of cubosomes [15,42,52,53]. Here we note that in our study we observed a small or negligible fraction of vesicles.

3.2. Imaging of the nanoparticles on hydrophobic surface liquid AFM

In addition to cryo-TEM, SSL-NPs were imaged with AFM on a hydrophobized silica surface in liquid mode in order to emulate their interaction with interfaces, which is relevant for delivery applications. [54] As it can be seen in Fig. 3, the nanoparticles are generally 30–60 nm in height and 250–600 nm in diameter. The fact that the diameter is much larger than we have observed both with DLS and cryo-TEM, indicates that the cubosomes partly spread on the surface and adopt a flatter conformation.

3.3. Stability of the nanoparticles in water

The shelf-life presents a critical feature of a formulation, therefore understanding the colloidal stability over time is fundamental in applying these aggregates as drug carriers. The cubosomes dispersion colloidal stability over time has been investigated by DLS and the results are summarized in Fig. 4. Both formulations are stable in terms of apparent hydrodynamic diameter and polydispersity index for at least 42 days at room temperature. These results show that both TMP and SSL extracts are stabilizing the lipid-water interface is such a way that they provide colloidal stability of the dispersion and preventing the system from flocculating.

3.4. Effect of physiological environment

The application of cubosomes for drug delivery and other biomedical

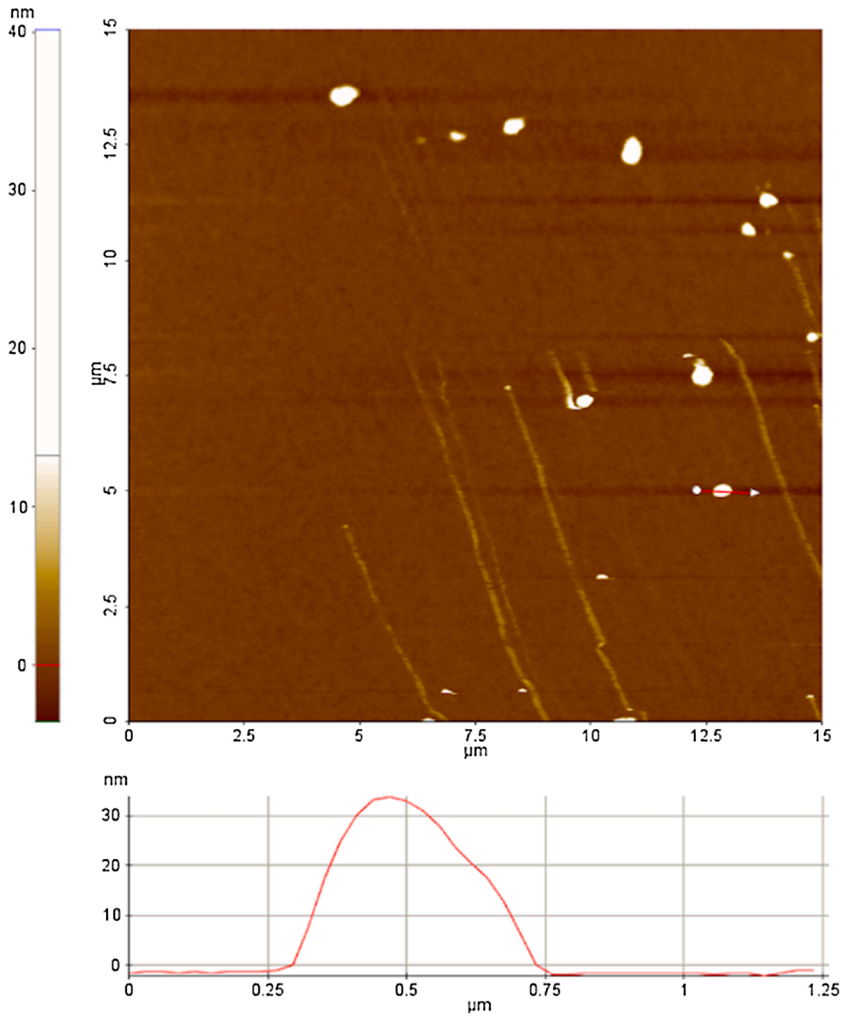

Fig. 3. AFM images of SSL-NPs on hydrophobic silica in liquid obtained in tapping mode.

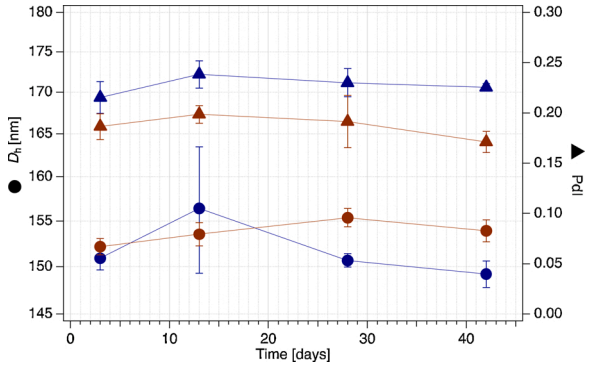

Fig. 4. Hydrodynamic diameter (circles) and polydispersity (triangles) over time of TMP-NPs (dark blue) and SSL-NPs (brown).

applications make their colloidal and structural stability in a physiological environment a crucial requirement. Indeed, pH and salt concentration can affect lipid self-assembly in terms of size, charge and structure. [55] Taking these factors into account, 10 mM phosphate saline buffer (PBS) pH 7.4 has been used to mimic the physiological environment.

First, an aliquot of the formulations was diluted 500 times in PBS in order to follow the changes in the size and polydispersity of the nanoparticles under these conditions. The size of the nanoparticles of both formulations increases significantly (to 250 nm) at the start of the incubation but remains stable in case of SSL-NPs (Fig. 5B). However, the size of the TMP-NPs continues to increase for the next two hours until it reaches 400 nm. The polydispersity is relatively stable in SSL-stabilized sample over the whole investigated time span, while it increases from 0.15 to 0.25 during the first 3 h in the TMP-stabilized formulation. These changes might indicate aggregation of particles due to screening effect caused by increasing the ionic strength with the added buffer.

Indeed, the electrophoretic mobility measurements showed that the negative potential has decreased significantly explaining the reduction of the cubosome colloidal stability, which in particular for TMP-NPs causes aggregation (see Table 3).

The effect of PBS on the internal structure of the two GGMs stabilized cubosomes was evaluated through SAXS measurements. It has previously been reported that the change in ionic strength can trigger shift from one phase to another. [56,57]

Fig. 5A shows the scattering curves of the TMP- and SSL-stabilized samples after dilution in PBS buffer 0.1 times.

After dilution of the TMP-NPs formulation in PBS, we observed the formation of visible macroscopic aggregates in solution. This phenomenon could be related to the aggregation of GGM and, thereby, of the nanoparticles (due to the elevated ionic strength). After removal of these visible aggregates, the solution has been analyzed by means of SAXS, but the concentration of GMO and GGM has changed in the solution, therefore we would not expect Bragg peaks related to the presence of a bicontinuous cubic phase. The precipitation was observed with the SSL-

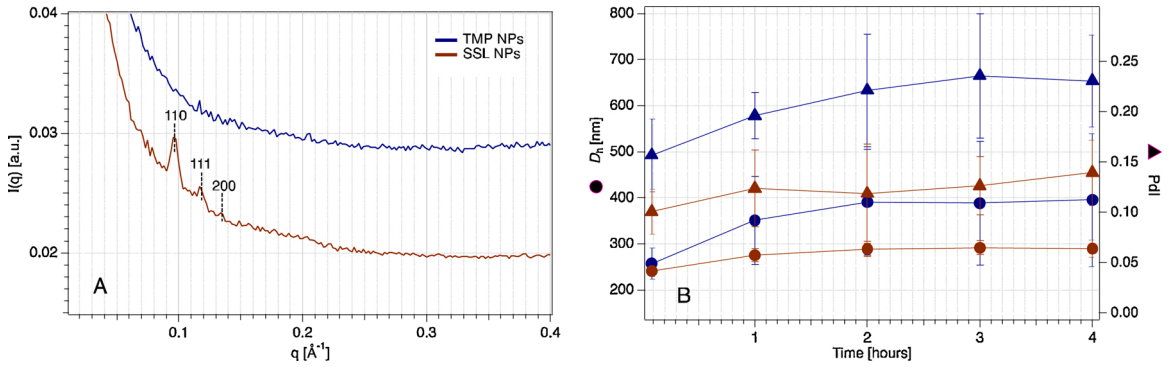

Fig. 5. SAXS curves of TMP-NPs (blue) and SSL-NPs (brown) seen in A and change in hydrodynamic diameter (circles) and polydispersity (triangles) seen in B in PBS buffer. The scattering curve of the TMP-NPs was shifted upwards by a factor of 0.01 for clarity.

Table 3
ζ-potential of TMP-NPs, SSL-NPs, as well as TMP and SSL extracts in PBS buffer determined at 25 °C.

Sample	ζ-potential ± SD [mV]
TMP-NPs	−0.9 ± 0.4
SSL-NPs	−7.4 ± 0.9
TMP	−1 ± 2
SSL	−6 ± 2

stabilized sample as well, however to a lower extent and the sample still appeared milky after dilution. Indeed, the SAXS patterns confirm that the SSL-NPs retained Pn3m phase with no significant change in terms of lattice parameter and water channel radius after addition of the PBS buffer. The lattice parameter and water channel radius of the SSL-NPs in PBS buffer was 93.1 ± 0.4 Å and 19.4 ± 0.1 Å, respectively. This is slightly smaller than the value for lattice parameter of 98.7 Å observed in water. On the other hand, the Bragg peaks completely disappear in case of the TMP-NPs indicating that it appears as if the internal structure is at least partly lost. Similar tendency was observed with DLS: due to a much lower concentration, the aggregation of the TMP-NPs could not be monitored beyond a size of 400 nm. The increase in terms of hydrodynamic diameter of both formulations (even though the increase is more pronounced in the case of the TMP-NPs) could be related to different factors. First, cations are adsorbed due to the apparent negative particles as can be observed from the reduction in the zeta potential values of the formulations in PBS. It should also be noted that the internal structure changes somewhat leading to a decrease in the lattice parameter. This can result in a partial aggregation of some of the particles that eventually causes precipitation of the TMP-NPs. We observed that the polydispersity increases as well. Here we note that for DLS measurements few of the larger aggregates have a relatively large influence on the mean size obtained. The effect is much smaller for the SSL-NPs. Preparing the particles directly in PBS instead of distilled did not work for the TMP-NPs and we wanted to compare the two hemicellulose samples.

The fact that the SSL-NPs formulation is more stable at an elevated ionic strength might be due to the higher ζ-potential as shown in Table 2. Moreover, a larger amount of monoolein is dispersed in the SSL-NPs sample than in the TMP-NPs one.

4. Conclusions

Softwood hemicellulose is an underutilized and abundant resource that can be used for a variety of applications thanks to its unique properties. [22,25,58–60] Its application as a stabilizer has already been proven in previous studies for oil-in-water emulsions. Indeed, other hemicelluloses such as xylan have found application in several fields, given their promising biological features. [61]

The ability of two softwood hemicellulose extracts, with different amount of lignin, to stabilize monoolein-based cubosomes was demonstrated in this study, where the higher lignin content in the SSL-extract facilitated stabilization of a larger fraction of the dispersed lipid phase. The presence of the hemicellulose extracts did not affect the self-assembly structure of monoolein in aqueous dispersions, giving a Pn3m bicontinuous cubic structure. Moreover, both formulations were stable over the period of at least 42 days with no significant changes in size or polydispersity. The results show that the physiological environment did not affect the structure for the SSL-stabilized cubosomes.

Indeed, the SSL-hemicellulose provided a better colloidal stability in comparison with the TMP-extract. This study shows that hemicellulose can be used as natural substitute to Pluronics to stabilize lipid liquid crystalline nanoparticles. Further studies are needed to reveal the biological effect of these aggregates, hence *in vitro* investigations will be performed as a future perspective.

CRediT authorship contribution statement

Polina Naidjonoka: Conceptualization, Investigation, Methodology, Data curation, Writing - original draft, Writing - review & editing. **Marco Fornasier:** Conceptualization, Investigation, Methodology, Data curation, Writing - original draft, Writing - review & editing. **David Pålsson:** Investigation, Data curation, Writing - review & editing. **Gregor Rudolph:** Investigation, Data curation, Writing - review & editing. **Basel Al-Rudainy:** Investigation, Data curation, Writing - review & editing. **Sergio Murgia:** Supervision, Writing - review & editing. **Tommy Nylander:** Resources, Supervision, Project administration, Writing - review & editing.

Declaration of Competing Interest

The authors declare no conflict of interest.

Acknowledgements

The research in this work was financed by BIOFUNC research project (supported by the Swedish Foundation for Strategic ResearchRBP14-0046) and FORMAS. The National Center for High Resolution Electron Microscopy, Lund University, is gratefully acknowledged for providing experimental resources. We also thank Anna Carnerup for the support provided during the cryo-TEM measurements. The PhD scholarship of M.F. was funded by the program POR-FSE Sardegna2014-2020.

Appendix A. Supplementary data

Supplementary material related to this article can be found, in the online version, at doi:https://doi.org/10.1016/j.colsurfb.2021.111753.

References

[1] H.M.G. Barriga, M.N. Holme, M.M. Stevens, Cubosomes: the next generation of smart lipid nanoparticles? Angew. Chem. Int. Ed. Engl. 58 (10) (2019) 2958–2978, https://doi.org/10.1002/anie.201804067.

[2] C. Neto, G. Aloisi, P. Baglioni, K. Larsson, Imaging Soft matter with the atomic force microscope: cubosomes and hexosomes, J. Phys. Chem. B 103 (19) (1999) 3896–3899, https://doi.org/10.1021/jp984551b.

[3] V. Meli, C. Caltagirone, C. Sinico, F. Lai, A.M. Falchi, M. Monduzzi, M. Obiols-Rabasa, G. Picci, A. Rosa, J. Schmidt, Y. Talmon, S. Murgia, Theranostic hexosomes for Cancer treatments: an in vitro study, New J. Chem. 41 (4) (2017) 1558–1565, https://doi.org/10.1039/c6nj03232j.

[4] Y. Chen, A. Angelova, B. Angelov, M.M. Drechsler, V. Garamus, R. Willumeit-Römer, A. Zou, Sterically stabilized spongosomes for multidrug delivery of anticancer nanomedicines, J. Mater. Chem. B 3 (39) (2015) 7734–7744, https://doi.org/10.1039/C5TB01193K.

[5] J. Gilbert, M.K. Valldeperas, S. Dhayal, J. Barauskas, C. Dicko, T. Nylander, Immobilisation of β-Galactosidase within a lipid sponge phase: structure, stability and kinetics characterisation, Nanoscale 11 (44) (2019) 21291–21301, https://doi.org/10.1039/C9NR06675F.

[6] S. Murgia, S. Biffi, R. Mezzenga, Recent advances of non-lamellar lyotropic liquid crystalline nanoparticles in nanomedicine, Curr. Opin. Colloid Interface Sci. 48 (2020) 28–39, https://doi.org/10.1016/j.cocis.2020.03.006.

[7] R. Prajapati, S. Salentinig, A. Yaghmur, Temperature triggering of kinetically trapped self-assemblies in citrem-phospholipid nanoparticles, Chem. Phys. Lipids 216 (2018) 30–38, https://doi.org/10.1016/j.chemphyslip.2018.09.003.

[8] U. Bazylińska, J. Kulbacka, J. Schmidt, Y. Talmon, S. Murgia, Polymer-free cubosomes for simultaneous bioimaging and photodynamic action of photosensitizers in melanoma skin Cancer cells, J. Colloid Interface Sci. 522 (2018) 163–173, https://doi.org/10.1016/j.jcis.2018.03.063.

[9] S. Biffi, L. Andolfi, C. Caltagirone, C. Garrovo, A.M. Falchi, V. Lippolis, A. Lorenzon, P. Macor, V. Meli, M. Monduzzi, M. Obiols-Rabasa, L. Petrizza, L. Prodi, A. Rosa, J. Schmidt, Y. Talmon, S. Murgia, Cubosomes forin vivofluorescence lifetime imaging, Nanotechnology 28 (5) (2016), https://doi.org/10.1088/1361-6528/28/5/055102, 055102.

[10] S. Murgia, A.M. Falchi, V. Meli, K. Schillén, V. Lippolis, M. Monduzzi, A. Rosa, J. Schmidt, Y. Talmon, R. Bizzarri, C. Caltagirone, Cubosome formulations stabilized by a dansyl-conjugated block copolymer for possible nanomedicine applications, Colloids Surf. B Biointerfaces 129 (2015) 87–94, https://doi.org/10.1016/j.colsurfb.2015.03.025.

[11] N. Alcaraz, Q. Liu, E. Hanssen, A. Johnston, B.J. Boyd, Clickable cubosomes for antibody-free drug targeting and imaging applications, Bioconjugate Chem. 29 (1) (2018) 149–157, https://doi.org/10.1021/acs.bioconjchem.7b00659.

[12] L. Boge, A. Umerska, N. Matougui, H. Bysell, L. Ringstad, M. Davoudi, J. Eriksson, K. Edwards, M. Andersson, Cubosomes post-loaded with antimicrobial peptides: characterization, bactericidal effect and proteolytic stability, Int. J. Pharm. 526 (1) (2017) 400–412, https://doi.org/10.1016/j.ijpharm.2017.04.082.

[13] M. Mendozza, C. Montis, L. Caselli, M. Wolf, P. Baglioni, D. Berti, On the thermotropic and magnetotropic phase behavior of lipid liquid crystals containing magnetic nanoparticles, Nanoscale 10 (7) (2018) 3480–3488, https://doi.org/10.1039/C7NR08478A.

[14] I.D.M. Azmi, P.P. Wibroe, L.-P. Wu, A.I. Kazem, H. Amenitsch, S.M. Moghimi, A. Yaghmur, A structurally diverse library of safe-by-design citrem-phospholipid lamellar and non-lamellar liquid crystalline nano-assemblies, J. Control. Release 239 (2016) 1–9, https://doi.org/10.1016/j.jconrel.2016.08.011.

[15] M. Fornasier, S. Biffi, B. Bortot, P. Macor, A. Manhart, F.R. Wurm, S. Murgia, Cubosomes stabilized by a polyphosphoester-analog of pluronic F127 with reduced cytotoxicity, J. Colloid Interface Sci. 580 (2020) 286–297, https://doi.org/10.1016/j.jcis.2020.07.038.

[16] M. Uyama, M. Nakano, J. Yamashita, T. Handa, Useful modified cellulose polymers as new emulsifiers of cubosomes, Langmuir 25 (8) (2009) 4336–4338, https://doi.org/10.1021/la900386q.

[17] M. Almgren, J. Borné, E. Feitosa, A. Khan, B. Lindman, Dispersed lipid liquid crystalline phases stabilized by a hydrophobically modified cellulose, Langmuir 23 (5) (2007) 2768–2777, https://doi.org/10.1021/la062482j.

[18] P.T. Spicer, W.B. Small, W.B. Small, M.L. Lynch, J.L. Burns, Dry powder precursors of cubic liquid crystalline nanoparticles (Cubosomes), J. Nanoparticle Res. 4 (4) (2002) 297–311, https://doi.org/10.1023/A:1021184216308.

[19] D. Fengel, G. Wegener, Wood: Chemistry, Ultrastructure, Reactions, Walter de Gruyter, 2011.

[20] K.S. Mikkonen, C. Xu, C. Berton-Carabin, K. Schroën, Spruce galactoglucomannans in rapeseed oil-in-Water emulsions: efficient stabilization performance and structural partitioning, Food Hydrocoll. 52 (2016) 615–624, https://doi.org/10.1016/j.foodhyd.2015.08.009.

[21] M. Bhattarai, F. Valoppi, S.-P. Hirvonen, S. Hietala, P. Kilpeläinen, V. Aseyev, K. S. Mikkonen, Time-dependent self-association of spruce galactoglucomannans depends on PH and mechanical shearing, Food Hydrocoll. 102 (2020), 105607, https://doi.org/10.1016/j.foodhyd.2019.105607.

[22] F. Valoppi, M.H. Lahtinen, M.J. Bhattarai, S.K. Kirjoranta, V.J. Juntti, L. Peltonen, P.O. Kilpeläinen, K.S. Mikkonen, Centrifugal fractionation of softwood extracts improves the biorefinery workflow and yields functional emulsifiers, Green Chem. 21 (17) (2019) 4691–4705, https://doi.org/10.1039/C9GC02007A.

[23] M.H. Lahtinen, F. Valoppi, V. Juntti, S. Heikkinen, P.O. Kilpeläinen, N.H. Maina, K. S. Mikkonen, Lignin-rich PHWE hemicellulose extracts responsible for extended emulsion stabilization, Front. Chem. 7 (2019), https://doi.org/10.3389/fchem.2019.00871.

[24] M. Lehtonen, M. Merinen, P.O. Kilpeläinen, C. Xu, S.M. Willför, K.S. Mikkonen, Phenolic residues in spruce galactoglucomannans improve stabilization of oil-in-Water emulsions, J. Colloid Interface Sci. 512 (2018) 536–547, https://doi.org/10.1016/j.jcis.2017.10.097.

[25] K.S. Mikkonen, S. Kirjoranta, C. Xu, J. Hemming, A. Pranovich, M. Bhattarai, L. Peltonen, P. Kilpeläinen, N. Maina, M. Tenkanen, M. Lehtonen, S. Willför, Environmentally-compatible alkyd paints stabilized by wood hemicelluloses, Ind. Crops Prod. 133 (2019) 212–220, https://doi.org/10.1016/j.indcrop.2019.03.017.

[26] J. Lundqvist, A. Teleman, L. Junel, G. Zacchi, O. Dahlman, F. Tjerneld, H. Stålbrand, Isolation and characterization of galactoglucomannan from spruce (Picea Abies), Carbohydr. Polym. 48 (1) (2002) 29–39, https://doi.org/10.1016/S0144-8617(01)00210-7.

[27] T. Hannuksela, M. Tenkanen, B. Holmbom, Sorption of dissolved galactoglucomannans and galactomannans to bleached kraft pulp, Cellulose 9 (3) (2002) 251–261, https://doi.org/10.1023/A:1021178420580.

[28] Henrik Vibe Scheller, Peter Ulvskov, Hemicelluloses, Annu. Rev. Plant Biol. 61 (1) (2010) 263–289, https://doi.org/10.1146/annurev-arplant-042809-112315.

[29] S. Willför, R. Sjöholm, C. Laine, M. Roslund, J. Hemming, B. Holmbom, Characterisation of water-soluble galactoglucomannans from Norway Spruce Wood and thermomechanical pulp, Carbohydr. Polym. 52 (2) (2003) 175–187, https://doi.org/10.1016/S0144-8617(02)00288-6.

[30] M. Rinne, O. Kautto, K. Kuoppala, S. Ahvenjärvi, V. Kitunen, H. Ilvesniemi, S. Wilför, R. Sormunen-Cristian, Digestion of wood-based hemicellulose extracts as screened by in vitro gas production method and verified in vivo using sheep, Agric. Food Sci. 25 (1) (2016), https://doi.org/10.23986/afsci.46502, 13-21-13–21.

[31] V. Deloule, C. Boisset, D. Hannani, A. Suau, A. Le Gouellec, J. Chroboczek, C. Botté, Y. Yamaryo-Botté, C. Chirat, B. Toussaint, Prebiotic role of softwood hemicellulose in healthy mice model, J. Funct. Foods 64 (2020), 103688, https://doi.org/10.1016/j.jff.2019.103688.

[32] L. Pitkänen, M.S. Heinonen, K. Mikkonen, Safety considerations of plant polysaccharides for food use: a case study on phenolic-rich softwood galactoglucomannan extract, Food Funct. 9 (4) (2018) 1931–1943, https://doi.org/10.1039/C7FO01425B.

[33] J. Thuvander, A.-S.E. Jönsson, Xtraction of galactoglucomannan from thermomechanical pulp mill process water by microfiltration and ultrafiltration—influence of microfiltration membrane pore size on ultrafiltration performance, Chem. Eng. Res. Des. 105 (2016) 171–176, https://doi.org/10.1016/j.cherd.2015.12.003.

[34] D. Zasadowski, J. Yang, H. Edlund, M. Norgren, Antisolvent precipitation of water-soluble hemicelluloses from TMP process water, Carbohydr. Polym. 113 (2014) 411–419, https://doi.org/10.1016/j.carbpol.2014.07.033.

[35] Biomass Compositional Analysis Laboratory Procedures | Bioenergy | NREL https://www.nrel.gov/bioenergy/biomass-compositional-analysis.html (accessed Oct 15, 2020).

[36] B. Al-Rudainy, M. Galbe, H. Schagerlöf, O. Wallberg, Antisolvent precipitation of hemicelluloses, Lignosulfonates and their complexes from ultrafiltrated spent sulfite liquor (SSL), Holzforschung 72 (10) (2018) 839–850, https://doi.org/10.1515/hf-2017-0218.

[37] T.E. Timell, Recent progress in the chemistry of wood hemicelluloses, Wood Sci. Technol. 1 (1) (1967) 45–70, https://doi.org/10.1007/BF00592255.

[38] J. Berglund, S. Azhar, M. Lawoko, M. Lindström, F. Vilaplana, J. Wohlert, G. Henriksson, The structure of galactoglucomannan impacts the degradation under alkaline conditions, Cellulose 26 (3) (2019) 2155–2175, https://doi.org/10.1007/s10570-018-1737-z.

[39] H. Krawczyk, A.-S. Jönsson, Separation of Dispersed Substances and Galactoglucomannan in Thermomechanical Pulp Process Water by Microfiltration, Sep. Purif. Technol. 79 (1) (2011) 43–49, https://doi.org/10.1016/j.seppur.2011.03.009.

[40] C.V. Kulkarni, W. Wachter, G. Iglesias-Salto, S. Engelskirchen, S. Ahualli, Monoolein: a magic lipid? Phys. Chem. Chem. Phys. 13 (8) (2011) 3004–3021, https://doi.org/10.1039/C0CP01539C.

[41] Gwyddion – Free SPM (AFM, SNOM/NSOM, STM, MFM, …) data analysis software http://gwyddion.net/ (accessed Oct 29, 2020).

[42] S.P. Akhlaghi, I.R. Ribeiro, B.J. Boyd, W. Loh, Impact of preparation method and variables on the internal structure, morphology, and presence of liposomes in phytantriol-pluronic(®) F127 cubosomes, Colloids Surf. B Biointerfaces 145 (2016) 845–853, https://doi.org/10.1016/j.colsurfb.2016.05.091.

[43] J.-Y. Kim, M.-G. Song, J.-D. Kim, Zeta Potential of Nanobubbles Generated by Ultrasonication in Aqueous Alkyl Polyglycoside Solutions, J. Colloid Interface Sci. 223 (2) (2000) 285–291, https://doi.org/10.1006/jcis.1999.6663.

[44] K.S. Mikkonen, D. Merger, P. Kilpeläinen, L. Murtomäki, U.S. Schmidt, M. Wilhelm, Determination of physical emulsion stabilization mechanisms of wood hemicelluloses via rheological and interfacial characterization, Soft Matter 12 (42) (2016) 8690–8700, https://doi.org/10.1039/C6SM01557C.

[45] H. Qiu, M. Caffrey, The phase diagram of the Monoolein/Water system: metastability and equilibrium aspects, Biomaterials 21 (3) (2000) 223–234, https://doi.org/10.1016/S0142-9612(99)00126-X.

[46] M. Nakano, A. Sugita, H. Matsuoka, T. Handa, Small-angle X-Ray scattering and 13C NMR investigation on the internal structure of "Cubosomes.", Langmuir 17 (13) (2001) 3917–3922, https://doi.org/10.1021/la010224a.

[47] P. Naidjonoka, M.K. Arcos Hernandez, G. Pálsson, F. Heinrich, H. Stålbrand, T. Nylander, On the interaction of Softwood Hemicellulose with cellulose surfaces in relation to molecular structure and physicochemical properties of hemicellulose, Soft Matter (2020), https://doi.org/10.1039/D0SM00264J.

[48] S. Aleandri, R. Mezzenga, The physics of lipidic mesophase delivery systems, Phys. Today 73 (2020) 38–44, https://doi.org/10.1063/PT.3.4522.

[49] C. Caltagirone, A.M. Falchi, S. Lampis, V. Lippolis, V. Meli, M. Monduzzi, L. Prodi, J. Schmidt, M. Sgarzi, Y. Talmon, R. Bizzarri, S. Murgia, Cancer-cell-Targeted theranostic cubosomes, Langmuir 30 (21) (2014) 6228–6236, https://doi.org/10.1021/la501332u.

[50] S. Murgia, A.M. Falchi, M. Mano, S. Lampis, R. Angius, A.M. Carnerup, J. Schmidt, G. Diaz, M. Giacca, Y. Talmon, M. Monduzzi, Nanoparticles from lipid-based liquid crystals: emulsifier influence on morphology and cytotoxicity, J. Phys. Chem. B 114 (10) (2010) 3518–3525, https://doi.org/10.1021/jp9098655.

[51] S. Kishani, F. Vilaplana, W. Xu, C. Xu, L. Wågberg, Solubility of softwood hemicelluloses, Biomacromolecules 19 (4) (2018) 1245–1255, https://doi.org/10.1021/acs.biomac.8b00088.

[52] S. Murgia, S. Bonacchi, A.M. Falchi, S. Lampis, V. Lippolis, V. Meli, M. Monduzzi, L. Prodi, J. Schmidt, Y. Talmon, C. Caltagirone, Drug-loaded fluorescent cubosomes: versatile nanoparticles for potential theranostic applications, Langmuir 29 (22) (2013) 6673–6679, https://doi.org/10.1021/la401047a.

[53] S. Jenni, G. Picci, M. Fornasier, M. Mamusa, J. Schmidt, Y. Talmon, A. Sour, V. Heitz, S. Murgia, C. Caltagirone, Multifunctional Cubic Liquid Crystalline Nanoparticles for Chemo- and Photodynamic Synergistic Cancer Therapy, Photochem. Photobiol. Sci. 19 (5) (2020) 674–680, https://doi.org/10.1039/C9PP00449A.

[54] D.P. Chang, J. Barauskas, A.P. Dabkowska, M. Wadsäter, F. Tiberg, T. Nylander, Non-lamellar lipid liquid crystalline structures at interfaces, Adv. Colloid Interface Sci. 222 (2015) 135–147, https://doi.org/10.1016/j.cis.2014.11.003.

[55] Q. Liu, Y.-D. Dong, T.L. Hanley, B.J. Boyd, Sensitivity of Nanostructure in Charged Cubosomes to Phase Changes Triggered by Ionic Species in Solution, Langmuir 29 (46) (2013) 14265–14273, https://doi.org/10.1021/la402426y.

[56] B.W. Muir, G. Zhen, P. Gunatillake, P.G. Hartley, Salt induced lamellar to bicontinuous cubic phase transitions in cationic nanoparticles, J. Phys. Chem. B 116 (11) (2012) 3551–3556, https://doi.org/10.1021/jp300239g.

[57] T.E. Hartnett, K. Ladewig, A.J. O'Connor, P.G. Hartley, K.M. McLean, Size and phase control of cubic lyotropic liquid crystal nanoparticles, J. Phys. Chem. B 118 (26) (2014) 7430–7439, https://doi.org/10.1021/jp502898a.

[58] J. Hartman, A.C. Albertsson, M.S. Lindblad, J. Sjöberg, Oxygen barrier materials from renewable sources: material properties of softwood hemicellulose-based films, J. Appl. Polym. Sci. 100 (4) (2006) 2985–2991, https://doi.org/10.1002/app.22958.

[59] K.S. Mikkonen, M. Tenkanen, P. Cooke, C. Xu, H. Rita, S. Willför, B. Holmbom, K. B. Hicks, M.P. Yadav, Mannans as stabilizers of oil-in-Water beverage emulsions, Lwt - Food Sci. Technol. 42 (4) (2009) 849–855, https://doi.org/10.1016/j.lwt.2008.11.010.

[60] S. Willför, K. Sundberg, M. Tenkanen, B. Holmbom, Spruce-derived mannans – a potential raw material for hydrocolloids and novel advanced natural materials, Carbohydr. Polym. 72 (2) (2008) 197–210, https://doi.org/10.1016/j.carbpol.2007.08.006.

[61] X. Li, X. Shi, M. Wang, Y. Du, Xylan chitosan conjugate - a potential food preservative, Food Chem. 126 (2) (2011) 520–525, https://doi.org/10.1016/j.foodchem.2010.11.037.